PHYSICAL REVIEW B **95**, 121102(R) (2017)

Correlated Dirac semimetallic state with unusual positive magnetoresistance in strain-free perovskite $SrIrO_3$

J. Fujioka,[1,2] T. Okawa,[1] A. Yamamoto,[3] and Y. Tokura[1,3]

[1]*Department of Applied Physics and Quantum-Phase Electronics Center (QPEC), University of Tokyo, Hongo, Tokyo 113-8656, Japan*

[2]*PRESTO, Japan Science and Technology Agency, Kawaguchi, Saitama 332-0012, Japan*

[3]*RIKEN Center for Emergent Matter Science (CEMS), Wako 351-0198, Japan*

(Received 23 September 2016; revised manuscript received 12 February 2017; published 3 March 2017)

We investigated magnetotransport properties and charge dynamics of strain-free perovskite $SrIrO_3$. Both the longitudinal and transverse magnetoresistivity (MR) are significantly enhanced with decreasing temperature, in accord with the evolution of the Dirac semimetallic state. The electron correlation effect in the Dirac state shows up as a dramatic change in charge dynamics with temperature and as an enhanced paramagnetic susceptibility. We propose that the field-induced topological transition of the Dirac node coupled to the enhanced paramagnetism causes the unique MR of correlated Dirac electrons.

DOI: 10.1103/PhysRevB.95.121102

Magnetoresistivity (MR) is one of the sensitive probes of the electronic structure in a solid and also leads to a potential application in magnetic memory and spintronics devices. For these decades, giant negative MR in multilayer magnetic materials and colossal negative MR in correlated electron systems have been extensively explored for practical applications [1,2], but it is only recently that positive MR in nonmagnetic semiconductors or semimetals has received renewed interest, along with rapidly growing research on topological semimetals [3–7]. Specifically, in three-dimensional Dirac semimetals such as Cd_3As_2, it is found that the MR is positive and nonsaturating up to a high magnetic field region in the transverse geometry, i.e., the electric current (I) perpendicular to the magnetic field B, but is negative in the longitudinal geometry ($B \parallel I$). Although the origin of unusual MR is still under debate, it is proposed that the field-induced topological transition of Dirac nodes, the impurity scattering of Dirac electrons [8,9], or the emergence of an axial current cause the unusual magnetotransport property [4,10–12]. Besides these one-electron band semimetals, it is argued that the Dirac or Weyl electrons can emerge in strongly correlated electron systems. One remarkable feature of correlated electron systems is that the electronic structure can be strongly coupled to the ordering or collective fluctuation of charge, spin, and orbital degrees of freedom. However, the charge transport/dynamics inherent in correlated Dirac/Weyl electrons remain almost unexplored experimentally, except for a few recent studies [13–15].

The perovskite $AIrO_3$ (A = Sr, Ca) provides a fertile playground to study the correlated Dirac electron. Due to the interplay between relativistic spin-orbit coupling and electron correlation, the electronic state near the Fermi energy (E_F) is mainly composed of a nearly half-filled $j_{\rm eff} = \frac{1}{2}$ multiplet of $5d$ orbitals of the Ir^{4+} ion, leading to a semimetallic state with a few electron and hole pockets [16–18]. Specifically, angle-resolved photoemission spectroscopy (ARPES) on epitaxial thin films has revealed an electron pocket with a Dirac-like dispersion at $(\pi/2,\pi/2)$ as well as two hole pockets with a quadratic band dispersion at $(\pi,0)$ and (π,π) in the thin-film sample [18]. Moreover, a theoretical study has predicted that the topological transition into a Weyl (semi)metal, nodal semimetal, or gapped state can be induced by applying a magnetic field along specific crystal orientations [19]. Such topological transitions of correlated Dirac electrons would manifest themselves as unusual magnetotransport properties, yet the magnetoresistivity for epitaxial thin-film samples is small and appears to be similar to that for conventional metals [20–23]. Moreover, a recent simulation study argues that the Dirac node is amenable to epitaxial strain and is gapped out by lattice distortion, which breaks the original orthorhombic crystal symmetry [24,25]. To overcome these issues, in this Rapid Communication, we have explored magnetotransport properties, magnetism, and charge dynamics for a strain-free bulk sample of perovskite $SrIrO_3$. Our results show that both transverse and longitudinal magnetoresistivity are dramatically enhanced with decreasing temperature. along with the evolution of the Dirac semimetallic state, and reaches as large as 100% and 50%, respectively, at 14 T and 2 K, which is two or three orders of magnitude larger than those observed in epitaxially strained thin films. We ascribe the unusual magnetoresistivity to the field-induced topological transition of the Dirac node.

Polycrystalline samples of $SrIrO_3$ were grown by a solid-state reaction under 5 GPa and 1000 °C by using a cubic-anvil-type facility [26]. High-pressure synthesis can provide samples which are composed of densely packed, large-size grains (1–10 μm) and are hence particularly suitable for magnetotransport and optical reflectance measurements (see also the Supplemental Material [27]). Resistivity, specific heat, and magnetization were measured by a physical (magnetization) property measurement system (Quantum Design). We measured optical reflectivity spectra by using a Fourier transform spectrometer (grating-type monochromator equipped with a microscope) in a photon energy region of 0.008–0.7 eV (0.5–5 eV), respectively. The reflectivity spectra in the energy region of 4–30 eV were measured at room temperature with the use of synchrotron radiation at UV-SOR, Institute for Molecular Science, Japan. The optical conductivity spectra were obtained by a Kramers-Kronig (KK) analysis with suitable extrapolation procedures.

Figures 1(a)–1(c) show the temperature dependence of the resistivity (ρ_{xx}), Hall coefficient (R_H), and Hall angle

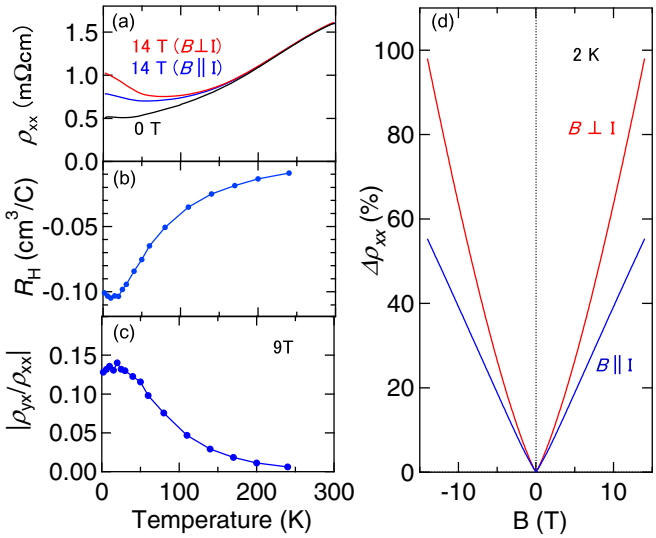

FIG. 1. Temperature dependence of (a) resistivity at 0 T (black) and 14 T (blue and red), (b) Hall coefficient, and (c) $|\rho_{yx}/\rho_{xx}|$ at 9 T, respectively. (d) Magnetoresistivity ratio defined by $[\rho_{xx}(B) - \rho_{xx}(0)]/\rho_{xx}(0)$ at 2 K.

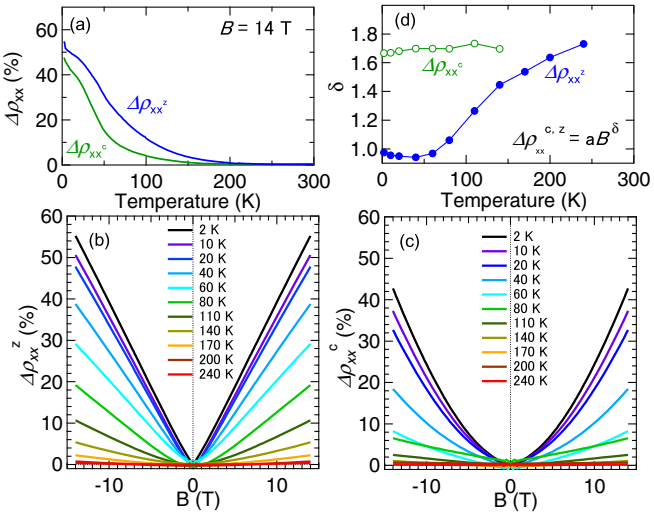

FIG. 2. Temperature dependence of $\Delta\rho^{z}_{xx}$ (blue) and $\Delta\rho^{c}_{xx}$ (green). Magnetic field dependence of (b) $\Delta\rho^{z}_{xx}$ and (c) $\Delta\rho^{c}_{xx}$. (d) The power law (δ) of the magnetoresistivity. The solid and open circles denote the δ of $\Delta\rho^{z}_{xx}$ and $\Delta\rho^{c}_{xx}$, respectively.

$|\rho_{yx}/\rho_{xx}|$, respectively. Both ρ_{xx} and R_H monotonically decrease with lowering temperature and are nearly temperature independent below 25 K. Simultaneously, $|\rho_{yx}/\rho_{xx}|$ is monotonically enhanced and reaches as large as 0.13 at 9 T and 20 K. Therefore, it is likely that the charge transport is governed by Dirac electrons rather than holes with a quadratic band dispersion at low temperatures.

In Fig. 1(a), we also show the resistivity at $B = 14$ T in both transverse and longitudinal geometries. In both geometries, the resistivity curves show an upturn and a clear MR is discerned below 150 K, which is qualitatively consistent with a previous study [26]. In Fig. 1(d), we show the MR ratio, i.e., $\Delta\rho_{xx} = [\rho_{xx}(B) - \rho_{xx}(0)]/\rho_{xx}(0)$ at 2 K. The longitudinal MR is B linear within the measured field range and exceeds 50% at 14 T, whereas the transverse MR is more B quadratic and reaches nearly 100% at 14 T. In general, the longitudinal MR is attributed to the spin-dependent mechanism as represented by the Zeeman splitting of bands (ρ^{z}_{xx}), whereas the transverse MR involves a contribution from the cyclotron motion of the electron (ρ^{c}_{xx}) as well. Given that the Matthiessen law is valid in the present case, ρ^{c}_{xx} may be derived by subtracting the longitudinal MR ($= \rho^{z}_{xx}$) from the transverse MR, i.e., $\rho^{c}_{xx} = \rho_{B\perp I} - \rho_{B\parallel I}$ [28]. Figure 2(a) shows the temperature dependence of MR ratios ($\Delta\rho^{z}_{xx}$ and $\Delta\rho^{c}_{xx}$) at 14 T. With decreasing temperature, $\Delta\rho^{c}_{xx}$ gradually increases below 150 K and rapidly grows around ~50 K, whereas $\Delta\rho^{z}_{xx}$ increases more moderately below 150 K. We note that $\Delta\rho^{z}_{xx}$ is nearly comparable or even larger than $\Delta\rho^{c}_{xx}$ in the entire temperature range. This is distinct from the case of conventional Dirac semimetals; therein, $\Delta\rho^{c}_{xx}$ is much larger than $\Delta\rho^{z}_{xx}$ in similar B and T regimes.

Figures 2(b) and 2(c) show the magnetic field dependence of $\Delta\rho^{z}_{xx}$ and $\Delta\rho^{c}_{xx}$ at various temperatures, respectively. The $\Delta\rho^{z}_{xx}$ is B linear at low temperatures, but tends to be more quadratic at higher temperatures. Meanwhile, $\Delta\rho^{c}_{xx}$ appears to be quadratic in the entire temperature range. To quantify the characteristic temperature, where the B dependence of MR changes, we fit the MR ratio by the empirical formula $\Delta\rho_{xx}(B) = aB^{\delta}$ with fitting parameters a and δ. Figure 2(d) displays the temperature dependence of δ. Here, δ of $\Delta\rho^{z}_{xx}$ is nearly unity below ~70 K ($= T^{*}$), but rapidly grows with increasing temperature. Alternatively, δ of $\Delta\rho^{c}_{xx}$ remains at about 1.7 at all analyzed temperatures.

To further look into the origin of the unique temperature variation of magnetoresistivity, we explored the charge dynamics by the optical conductivity spectra. Figure 3(a) shows the optical conductivity spectra at 300 and 10 K. Both spectra show two broad peak structures around 0.13 eV (α) and 0.67 eV (β), respectively, except for the sharp peaks due to optical phonon modes below 0.08 eV. As schematically shown in the inset to Fig. 3(a), we have assigned these peaks as the optical transition from an occupied $j_{\rm eff} = \frac{1}{2}$ state to an unoccupied $j_{\rm eff} = \frac{1}{2}$ state, and that from an occupied $j_{\rm eff} = \frac{3}{2}$ state to an unoccupied $j_{\rm eff} = \frac{1}{2}$ state, respectively. Similar peak structures are observed in $Sr_3Ir_2O_7$, Sr_2IrO_4, and a thin film of $SrIrO_3$ [29,30], and are partly consistent with the prediction by dynamical mean field theory albeit the absence of an α peak in the theory [16]. Although the β peak appears to be nearly temperature independent, the spectral shape of the α peak at 300 K is significantly different from that at 10 K. Figure 3(b) shows a magnified view of the optical conductivity spectra in the low-energy region. Some phonon modes are subject to the Fano resonance effect due to the overlapping electronic continuum, yet no major change is discerned, indicating that the structural symmetry remains intact in the entire temperature regime. At 300 K, the optical conductivity spectra are nearly flat below 0.1 eV, which is characteristic of an incoherent metal state in a correlated electron system [31]. With decreasing temperature, the spectral intensity of the electronic continuum below 0.11 eV is dramatically reduced down to as small as 130 Ω^{-1} cm^{-1} at 10 K, apart from the tail of the Drude response below 0.02 eV. Furthermore, one can see

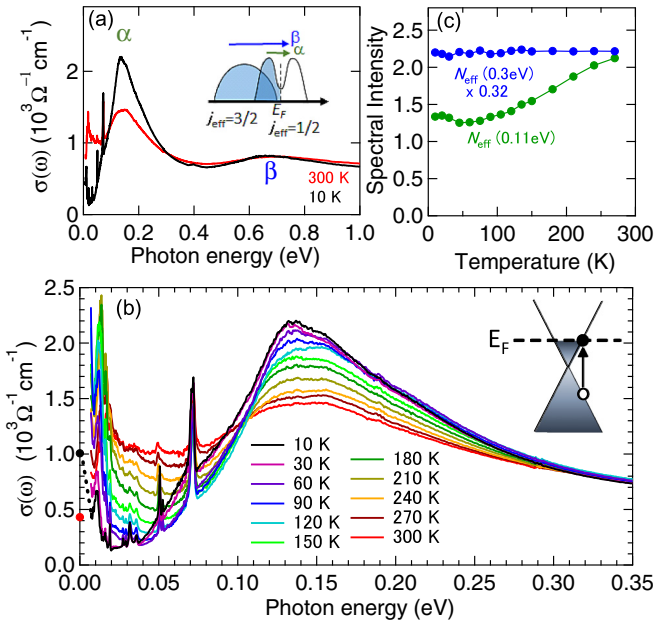

FIG. 3. (a) The optical conductivity spectra at 300 and 10 K. The inset shows the schematic picture of the density of states for $j_{\rm eff} = \frac{1}{2}$ and $j_{\rm eff} = \frac{3}{2}$ manifolds. (b) Magnified view of optical conductivity spectra below 0.35 eV. The circles (black: 10 K; red: 300 K) and dashed line denote the dc conductivity derived from resistivity measurements and the expected Drude response, respectively. Note that the sample for optical measurements is cut from a different batch, which is used for magnetotransport measurements; resistivity is nearly twice in the former. The inset denotes the schematic picture for the interband transition in the Dirac cone. (c) Temperature dependence of spectral intensity with cutoff energies of 0.11 and 0.3 eV. $N_{\rm eff}(\hbar\omega = 0.3$ eV) is multiplied by 0.32.

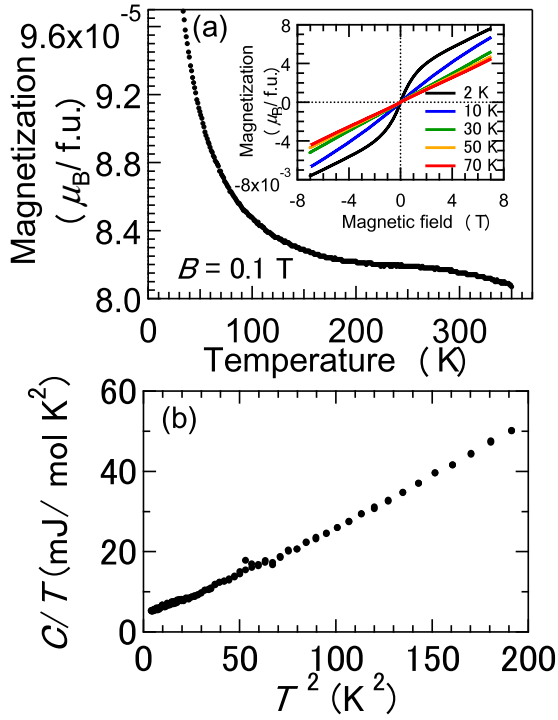

FIG. 4. (a) Temperature dependence of magnetization measured at 0.1 T. The inset shows the magnetic field dependence of magnetization at various temperatures. (b) T^2 dependence of specific heat (C) data divided by temperature (T).

an absorption edge around 0.06 eV with a quasilinearly rising part above 0.09 eV and a notchlike structure at 0.13 eV. Such spectral features are commonly observed in conventional Dirac semimetals and are attributed to the threshold of the interband transition of the Dirac cone [in the inset to Fig. 3(b)] and to the van Hove singularity of the band structure [32,33]. Given that the absorption edge is equal to twice the Fermi energy ($E_{\rm F}$), namely, that the Dirac cone is nearly particle-hole symmetric in the relevant energy scale [18], $E_{\rm F}$ is estimated to be about 30 ± 5 meV, which is smaller than the reported value for the epitaxial thin film, or closer to the Dirac node. Furthermore, by assuming a Fermi velocity $v_{\rm F} = 1.2 \times 10^5$ m/s [18], the density of the Dirac electron is estimated to be around $(7 \pm 4) \times 10^{18}$ cm^{-3}. Although this value is slightly smaller than that derived by the Hall coefficient (3×10^{19} cm^{-3}) on the basis of a single carrier model, the overall spectral feature suggests that the low-energy charge excitation is mostly governed by the Dirac electrons, with the least contribution coming from the possibly coexisting hole pocket(s). To further quantify the temperature variation of the spectral weight below 0.1 eV, we have calculated the effective number of electrons ($N_{\rm eff}$), defined as

$$N_{\rm eff}(\hbar\omega_c) = \frac{2m_0 V}{\pi e^2} \int_0^{\omega_c} \sigma(\omega) d\omega. \quad (1)$$

Here, m_0, V, and ω_c are the free-electron mass, cell volume, and cutoff energy, respectively. Figure 3(c) shows the temperature dependence of $N_{\rm eff}(\hbar\omega = 0.11$ eV) and $N_{\rm eff}(\hbar\omega = 0.3$ eV). As the temperature decreases, $N_{\rm eff}(\hbar\omega = 0.11$ eV) monotonically decreases and is nearly temperature independent below 70 K, which coincides with T^* (crossover temperature of MR). Since $N_{\rm eff}(\hbar\omega = 0.3$ eV) is nearly constant in the whole temperature region, the exhausted spectral weight below 0.11 eV is nearly compensated by the rapid growth of the α peak around 0.15 eV. Considering these results, it is anticipated that a significant reconstruction of the electronic structure with temperature mainly occurs in the occupied $j_{\rm eff} = \frac{1}{2}$ state and the $j_{\rm eff} = \frac{3}{2}$ state located near $E_{\rm F}$, while keeping intact the unoccupied $j_{\rm eff} = \frac{1}{2}$ state and the $j_{\rm eff} = \frac{3}{2}$ state located far from $E_{\rm F}$.

Such a large change in the electronic structure may impact the magnetism. Figure 4(a) displays the temperature dependence of magnetization measured at 0.1 T. As the temperature decreases from 350 K, the magnetization gradually increases, shows a plateau between 250 and 200 K, and then steeply increases at lower temperatures. There is no clear indication of a magnetic phase transition above 2 K and the magnetization field curve is linear as a function of the magnetic field except at 2 K, as shown in the inset to Fig. 4(a). To quantify the paramagnetic susceptibility, we fitted the inverse magnetic susceptibility (χ^{-1}) below 240 K by the Curie-Weiss law, defined as $[A/(T - \theta_{\rm W}) + \chi_{\rm p} + \chi_{\rm d}]^{-1}$. Here, A, $\theta_{\rm W}$, $\chi_{\rm p}$, and $\chi_{\rm d}$ are the Curie constant, Weiss temperature, paramagnetic susceptibility, and diamagnetic susceptibility of the core electrons, respectively. The $\theta_{\rm W}$ and $\chi_{\rm p}$ are estimated to be

0.3 K and 5.3×10^{-4} emu/mol, respectively. The small θ_W is in accord with the absence of magnetic ordering above 2 K. This is further confirmed by the temperature dependence of specific heat (C). Figure 4(b) shows the C/T plotted as a function of T^2. C/T linearly increases as a function of T^2 without any clear anomaly of the magnetic phase transition above 2 K. By assuming the relation $C/T = \gamma + \beta T^2$, where γ and β are the electronic specific coefficient and coefficient of the T^3 term, γ is estimated to be 4.4 mJ/mol K^2, yielding a Wilson ratio ($=3\pi^2 k_B^2 \chi_p/\mu_B^2\gamma$) of 8.8. This value is much larger than that of a paramagnetic Fermi liquid ($\sim$2) and indicates the presence of enhanced paramagnetism, which may originate from an instability of ferromagnetic ordering [34–36] or an enhancement of Van Vleck magnetism due to the nearly degenerate $j_{\text{eff}} = \frac{1}{2}$ and $j_{\text{eff}} = \frac{3}{2}$ manifolds located near E_F.

Taking these results into consideration, we discuss the origin of magnetoresistivity. On the basis of the temperature dependence of magnetoresistivity, charge dynamics, and magnetic susceptibility, it is likely that positive magnetoresistivity is enhanced along with the evolution of the Dirac semimetallic state and enhanced paramagnetism. Since our sample is of a polycrystalline form, the unusual magnetoresistivity might be attributed not only to the intrinsic bulk state but possibly also to the defects or the surface state at the grain boundary. Indeed, a large B-linear magnetoresistivity is often observed in heavily disordered materials, which can be simply explained by a classical model based on random resistor networks [37,38]. In such a case, however, the charge transport is incoherent even under zero magnetic field, which is not the case in the present system; the resistivity and optical conductivity spectra exhibit a metallic behavior and a sharp Drude response, respectively. Another possibility would be the Zeeman splitting coupled to the Landau levels of bulk Dirac electrons as observed in some Dirac semimetals [39]. However, this is again not likely the case, since the onset temperature of the Zeeman splitting term is higher than that of the cyclotron motion term in the present system. A more plausible scenario is the field-induced topological transition of a Dirac node. It is proposed that the Dirac semimetallic state with a topological surface state turns into the Weyl semimetal or a line-node semimetal via Zeeman coupling by applying the magnetic field along [100] and [010], but is gapped out under the magnetic field tilted away from the (001) plane [17,32]. Considering that each crystal grain in our polycrystalline sample is randomly oriented to the applied magnetic field, the gap opening may have the most dominant impact on transport among the possible topological transitions. Since enhanced paramagnetism may promote Zeeman splitting or mixing among the $j_{\text{eff}} = \frac{1}{2}$ and $j_{\text{eff}} = \frac{3}{2}$ states, it is conceivable that the topological transition with a reduction of transport relaxation time or the elimination of the topological surface state coupled to the bulk Dirac node is responsible for the unusually large positive magnetoresistivity observed, which is two or three orders of magnitude larger than in epitaxially strained thin films. Moreover, E_F appears to be more closely tuned to the Dirac node in the present strain-free bulk sample. Therefore, the removal of strain in the precisely half-filled-band condition should be important for further investigations on the interesting transport phenomena of correlated Dirac electrons, as in the present system; for example, negative longitudinal magnetoresistivity due to a chiral anomaly may show up in a single-crystal or strain-free thin film, when the Weyl semimetallic state is induced under a magnetic field directed precisely along [100].

In summary, we have investigated the magnetotransport and charge dynamics of correlated Dirac electrons in the strain-free perovskite $SrIrO_3$. Positive magnetoresistivity (MR) is dramatically enhanced at low temperatures in both transverse and longitudinal geometries. The longitudinal (transverse) MR is B linear (more B quadratic) and exceeds 50% (100%) at 14 T at 2 K, which is two or three orders of magnitude larger than in an epitaxially strained thin film of $SrIrO_3$. The optical conductivity spectra dramatically change on an energy scale of 0.3 eV, and an absorption structure due to the interband transition of the Dirac cone shows up below 100 K. Combined with the evolution of paramagnetic susceptibility, we propose that the field-induced topological transition of the Dirac node promoted by enhanced paramagnetism gives rise to the unique magnetoresistivity of correlated Dirac electrons in the present semimetal.

We thank N. Nagaosa and T. Arima for useful discussions. This work was partly supported by a Grant-In-Aid for Science Research (No. 24224009 and No. 16H00981) from the MEXT, and by PRESTO, JST, Japan.

[1] A. Fert, Rev. Mod. Phys. **80**, 1517 (2008).
[2] Y. Tokura and Y. Tomioka, J. Magn. Magn. Mater. **200**, 1 (1999).
[3] M. N. Ali, J. Xiong, S. Flynn, J. Tao, Q. D. Gibson, L. M. Schoop, T. Liang, N. Haldolaarachchige, M. Hirschberger, N. P. Ong, and R. J. Cava, Nature (London) **514**, 205 (2014).
[4] T. Liang, Q. Gibson, M. N. Ali, M. Liu, R. J. Cava, and N. P. Ong, Nat. Mater. **14**, 280 (2015).
[5] A. Narayanan, M. D. Watson, S. F. Blake, N. Bruyant, L. Drigo, Y. L. Chen, D. Prabhakaran, B. Yan, C. Felser, T. Kong, P. C. Canfield, and A. I. Coldea, Phys. Rev. Lett. **114**, 117201 (2015).
[6] X. Huang, L. Zhao, Y. Long, P. Wang, D. Chen, Z. Yang, H. Liang, M. Xue, H. Weng, Z. Fang, X. Dai, and G. Chen, Phys. Rev. X **5**, 031023 (2015).
[7] F. Y. Yang, K. Liu, K. Hong, D. H. Reich, P. C. Searson, and C. L. Chien, Science **284**, 1335 (1999).
[8] J. Klier, I. V. Gornyi, and A. D. Mirlin, Phys. Rev. B **92**, 205113 (2015).
[9] J. C. W. Song, G. Refael, and P. A. Lee, Phys. Rev. B **92**, 180204(R) (2015).
[10] J. Cao, S. Liang, C. Zhang, Y. Liu, J. Huang, Z. Jin, Z.-G. Chen, Z. Wang, Q. Wang, J. Zhao, S. Li, X. Dai, J. Zou, Z. Xia, L. Li, and F. Xiu, Nat. Commun. **6**, 7779 (2015).
[11] H. Li, H. He, H.-Z. Lu, H. Zhang, H. Liu, R. Ma, Z. Fan, S.-Q. Shen, and J. Wang, Nat. Commun. **7**, 10301 (2016).
[12] Z. J. Xiang, D. Zhao, Z. Jin, C. Shang, L. K. Ma, G. J. Ye, B. Lei, T. Wu, Z. C. Xia, and X. H. Chen, Phys. Rev. Lett. **115**, 226401 (2015).
[13] K. Ueda, J. Fujioka, B.-J. Yang, J. Shiogai, A. Tsukazaki, S. Nakamura, S. Awaji, N. Nagaosa, and Y. Tokura, Phys. Rev. Lett. **115**, 056402 (2015).

[14] Z. Tian, Y. Kohama, T. Tomita, H. Ishizuka, T. H. Hsieh, J. J. Ishikawa, K. Kindo, L. Balents, and S. Nakatsuji, Nat. Phys. **12**, 134 (2015).
[15] D. Liu, K. Ishikawa, R. Takehara, K. Miyagawa, M. Tamura, and K. Kanoda, Phys. Rev. Lett. **116**, 226401 (2016).
[16] H. Zhang, K. Haule, and D. Vanderbilt, Phys. Rev. Lett. **111**, 246402 (2013).
[17] J. M. Carter, V. V. Shankar, M. A. Zeb, and H.-Y. Kee, Phys. Rev. B **85**, 115105 (2012).
[18] Y. F. Nie, P. D. C. King, C. H. Kim, M. Uchida, H. I. Wei, B. D. Faeth, J. P. Ruf, J. P. C. Ruff, L. Xie, X. Pan, C. J. Fennie, D. G. Schlom, and K. M. Shen, Phys. Rev. Lett. **114**, 016401 (2015).
[19] Y. Chen, Y.-M. Lu, and H.-Y. Kee, Nat. Commun. **6**, 6593 (2015).
[20] L. Zhang, Y. B. Chen, B. Zhang, J. Zhou, S. Zhang, Z. Gu, S. Yao, and Y. F. Chen, J. Phys. Soc. Jpn. **83**, 054707 (2014).
[21] D. Hirai, J. Matsuno, D. Nishio-Hamane, and H. Takagi, Appl. Phys. Lett. **107**, 012104 (2015).
[22] J. H. Gruenewald, J. Nichols, J. Terzic, and G. Cao, J. Mater. Res. **29**, 2491 (2014).
[23] A. Biswas, K.-S. Kim, and Y. H. Jeong, J. Appl. Phys. **116**, 213704 (2014).
[24] Z. T. Liu, M. Y. Li, Q. F. Li, J. S. Liu, W. Li, H. F. Yang, Q. Yao, C. C. Fan, X. G. Wan, Z. Wang, and D. W. Shen, Sci. Rep. **6**, 30309 (2016).
[25] J. Liu, D. Kriegner, L. Horak, D. Puggioni, C. Rayan Serrao, R. Chen, D. Yi, C. Frontera, V. Holy, A. Vishwanath, J. M. Rondinelli, X. Marti, and R. Ramesh, Phys. Rev. B **93**, 085118 (2016).
[26] J. G. Zhao, L. X. Yang, Y. Yu, F. Y. Li, R. C. Yu, Z. Fang, L. C. Chen, and C. Q. Jin, J. Appl. Phys. **103**, 103706 (2008).
[27] See Supplemental Material at http://link.aps.org/supplemental/10.1103/PhysRevB.95.121102 for the sample characterization.
[28] J. M. Harris, Y. F. Yan, P. Matl, N. P. Ong, P. W. Anderson, T. Kimura, and K. Kitazawa, Phys. Rev. Lett. **75**, 1391 (1995).
[29] S. J. Moon, H. Jin, K. W. Kim, W. S. Choi, Y. S. Lee, J. Yu, G. Cao, A. Sumi, H. Funakubo, C. Bernhard, and T. W. Noh, Phys. Rev. Lett. **101**, 226402 (2008).
[30] H. J. Park, C. H. Sohn, D. W. Jeong, G. Cao, K. W. Kim, S. J. Moon, H. Jin, D.-Y. Cho, and T. W. Noh, Phys. Rev. B **89**, 155115 (2014).
[31] D. N. Basov, R. D. Averitt, D. van der Marel, M. Dressel, and K. Haule, Rev. Mod. Phys. **83**, 471 (2011).
[32] R. Y. Chen, S. J. Zhang, J. A. Schneeloch, C. Zhang, Q. Li, G. D. Gu, and N. L. Wang, Phys. Rev. B **92**, 075107 (2015).
[33] D. Neubauer, J. P. Carbotte, A. A. Nateprov, A. Lohle, M. Dressel, and A. V. Pronin, Phys. Rev. B **93**, 121202(R) (2016).
[34] K. Yamaura and E. Takayama-Muromachi, Phys. Rev. B **64**, 224424 (2001).
[35] G. Cao, V. Durairaj, S. Chikara, L. E. DeLong, S. Parkin, and P. Schlottmann, Phys. Rev. B **76**, 100402(R) (2007).
[36] K. Yoshimura, T. Imai, T. Kiyama, K. R. Thurber, A. W. Hunt, and K. Kosuge, Phys. Rev. Lett. **83**, 4397 (1999).
[37] R. Xu, A. Husmann, T. F. Rosenbaum, M.-L. Saboungi, J. E. Enderby, and P. B. Littlewood, Nature (London) **390**, 57 (1997).
[38] M. M. Parish and P. B. Littlewood, Nature (London) **426**, 162 (2003).
[39] C. M. Wang and X. L. Lei, Phys. Rev. B **86**, 035442 (2012).